Journal of Alloys and Compounds 509 (2011) 9565–9571

Contents lists available at ScienceDirect

Journal of Alloys and Compounds

journal homepage: www.elsevier.com/locate/jallcom

Surface and in-depth characterization of InGaN compounds synthesized by plasma-assisted molecular beam epitaxy

Mirosław Krawczyk[a,*], Wojciech Lisowski[a], Janusz W. Sobczak[a], Andrzej Kosiński[a], Aleksander Jablonski[a], Czesław Skierbiszewski[b], Marcin Siekacz[b], Sylwia Wiązkowska[b]

[a] Institute of Physical Chemistry, Polish Academy of Sciences, Kasprzaka 44/52, 01-224 Warszawa, Poland
[b] Institute of High Pressure Physics, Polish Academy of Sciences, Sokołowska 29/37, 01-142 Warszawa, Poland

ARTICLE INFO

Article history:
Received 23 May 2011
Accepted 19 July 2011
Available online 28 July 2011

Keywords:
Inorganic materials
Nitride materials
Crystal growth
Composition fluctuations
Photoelectron spectroscopies
X-ray diffraction

ABSTRACT

InGaN layers with multiple quantum wells are widely used as active layers in advanced optoelectronic devices. In the present work, surface properties of some InGaN layers grown on GaN/sapphire substrates by plasma-assisted molecular beam epitaxy were examined. The total indium content incorporated in the crystalline lattice of $In_{0.165}Ga_{0.835}N$ and $In_{0.353}Ga_{0.647}N$ layers grown with a thickness of 70–200 nm was controlled by the growth temperature, and was determined from X-ray diffraction. Auger electron spectroscopy and X-ray photoelectron spectroscopy analysis reveal relatively smaller concentration of In within the surface area than in the bulk of the InGaN layers. The Ar^+ XPS depth profile analysis shows the thick InGaN layers to be chemically homogeneous within an analytical area. To determine the electron inelastic mean free path in the layers within the 500–2000 eV range, relative elastic-peak electron spectroscopy measurements with Ni and Au standards were performed. The measured IMFPs were considerably larger than those predicted from the TPP-2M formula. The smallest root-mean-square-deviation and the mean percentage deviation of 9.9 Å and 44.5%, respectively, were found between EPES IMFP data and those predicted for the $In_{0.353}Ga_{0.647}N$ layer with respect to the Au standard. This work provided the detailed compositional and chemical changes of InGaN thick layers, and could be useful in solving key issues associated with the growth of high-quality layer with much higher In content.

1. Introduction

For the last decade, GaN and Ga-rich InGaN compounds have been successfully implemented in advanced photonic and optoelectronic devices operating in the blue and ultraviolet frequency range. In addition, indium gallium nitride is of special interest to the solar energy industry because of its highly tunable band gap, high heat capacity and low sensitivity to ionizing radiation [1]. It is already known that the low-temperature growth of the thick InGaN layer results in the low crystalline quality and the inhomogeneous distributions of In content in the layer [2]. Piner et al. [3] reported that indium droplets may form, which acts as sink for InN, preventing the low-temperature growth of InGaN layers with high In content. Indium droplet formation is a common problem in InGaN growth [4], especially in the In-rich InGaN layer. It reveals that formation of indium droplet can be seen as a way of indium loss. Furthermore, at low temperatures the crystalline quality of the layer is inferior at due to poor surface mobility of the ad-atoms, resulting in the three-dimensional growth. In addition, InGaN compounds suffer from phase separation because of the strain produced by large lattice mismatch (due to very different tetrahedral radii) between InN and GaN. Therefore, the large size difference between Ga and In atoms makes growth of $In_xGa_{1-x}N$, particularly for $x > 0.2$.

One of the widely discussed features of InGaN compounds is the compositional inhomogeneity, which is usually considered as a compositional fluctuation or phase separation in the alloy growth [5–8]. Based on X-ray diffraction (XRD) and optical absorption studies, Singh and co-workers [5] provided a strong evidence of phase separation in InGaN thick films grown by molecular beam epitaxy (MBE). These studies have shown that up to 30 at.% indium can be easily incorporated in InGaN bulk films. Further increase of the indium concentration results in phase separation of indium nitride. Chen et al. [9] observed the spontaneous formation of nanometer-size compositional inhomogeneities on InGaN (0 0 0 1) surfaces prepared by MBE. These surface structures consisted either vacancy islands or ordered vacancy rows. The spontaneous formation of such structures was shown to be driven by a significant strain in the surface layers, and by the relative weakness of the In–N bond compared to Ga–N. Theory indicates [9] that In will preferentially locate at the edges and interior of the structures, thereby giving rise to an inhomogeneous In distribution at the surface. Effects due to phase separation in InGaN were clearly identified [6] as

* Corresponding author.
E-mail address: mkrawczyk@ichf.edu.pl (M. Krawczyk).

0925-8388/$ – see front matter © 2011 Elsevier B.V. All rights reserved.
doi:10.1016/j.jallcom.2011.07.052

having major effects on the performance of devices, in particular light-emitting diodes (LEDs) and injection lasers.

Despite significant progress in InGaN technology, the fundamental studies on these materials are rather limited. In the published papers the physical and chemical properties of GaN and InN were mostly discussed [10–15]. Some recently published papers reviewed the fundamental properties of InGaN layers [14,16,17] and only few addressed the problems of thick InGaN layers with medium and high In contents [5,18].

It is known that the optical properties of InGaN-based semiconductors depend on their surface and sub-surface region properties. Generally, only the chemical composition is considered as an indicative surface factor. Nevertheless, it is still a lack of experimental data in which the chemical composition is correlated with the electron transport description within the surface area of such semiconductors.

The inelastic mean free path (IMFP) of electrons is a basic parameter for quantification of the surface-sensitive electron spectroscopies, e.g. Auger electron spectroscopy (AES) and X-ray photoelectron spectroscopy (XPS) [19]. This parameter is defined as the average of distances, measured along the trajectories, that electrons with a given energy travel between inelastic collisions in a substance [20,21]. Recent advances in quantitative AES and XPS analyses, and the important role of the IMFP in the accurate quantification of both techniques has been reviewed by Jablonski [19]. An extensive database of IMFP values in elements, and inorganic or organic compounds has been published [22]. However, the IMFPs for InGaN compounds are still lacking. They can be obtained from the NIST Database 71 [23] or calculated using the TPP-2M predictive formula [24], which is applicable for any solid. Moreover, IMFPs can be also measured experimentally by elastic-peak electron spectroscopy (EPES) [25,26]. Recently, EPES has been successfully used to measure the IMFPs in selected wide band-gap semiconductors, e.g., GaN [27], SiC [28] and $Cd_{0.88}Mn_{0.12}Te$ [29].

The relative EPES method requires the measurements of the elastic backscattering intensity from an examined material and from a reference, e.g. Ni, Cu, Ag, and Au, which are recommended for use as the reference materials [22]. Principles of relative EPES measurement procedures have already been described in detail elsewhere [26].

In this paper, we examined surface- and subsurface properties (chemical composition and its variation in depth, electron transport) of the two InGaN layers grown on GaN/sapphire substrates using a combination of AES, XPS and EPES. Application of these surface-sensitive analytical techniques allowed: (i) to detect the surface composition and chemistry of InGaN thick layers as-grown; (ii) to evaluate the influence of 2 keV Ar^+ ion-bombardment on the surface composition and chemistry of the layers; (iii) to find experimentally the IMFP of 500–2000 eV electrons in the examined layers.

2. Experimental details

2.1. Growth of InGaN compounds

The (70–200)-nm thick InGaN layers were deposited on Ga polarity (0 0 0 1) 3 μm thick GaN/sapphire substrates by plasma-assisted molecular beam epitaxy (PAMBE). The In-rich conditions were used to achieve high quality growth. The composition of the In content was controlled by growth temperature. Details of the PAMBE reactor, growth configuration, and the processing parameters were similar to those previously reported [30].

2.2. Characterization of bulk In content in InGaN compounds

X-ray diffraction (XRD) reciprocal space map analysis of two as-grown $In_xGa_{1-x}N$ compounds reveals the bulk In content x to be 16.5 and 35.3 at.%. These values agree well with the ellipsometric analysis data of the $In_xGa_{1-x}N$ energy gap (x = 20 and 34 at.%) [30]. The XRD reciprocal space mapping reveals also that these InGaN layers are relaxed. Details of both XRD and optical characterization techniques used here were published in Ref. [30].

2.3. Characterization of surface and subsurface In content in InGaN compounds

The as-grown InGaN samples were analysed *ex situ* in separate ultrahigh vacuum (UHV) systems using AES, XPS and EPES techniques.

The AES measurements were carried out using the MICROLAB 350 spectrometer (Thermo VG Scientific) with a spherical sector analyzer. The Auger spectra were taken at the normal incidence of the primary electron beam (E_p = 2 keV). AES quantification was based using the software Avantage (ver. 4.30, Thermo Fisher Scientific) on the Ga LMM (1064 eV), In MNN (404 eV) and N KVV (385 eV) peak intensities. The same spectrometer was also used in EPES measurements.

High-resolution XPS measurements were performed using a PHI 5000 VersaProbe™ spectrometer with microfocused and monochromatic Al K_α radiation. Details of the spectrometer and its arrangement were recently reported by Jablonski [31]. The spectrometer was equipped with a spherical capacitor energy analyzer with multi-channel detection within a 100 μm × 100 μm area for XPS analysis. The X-ray beam was incident at the surface at the angle of 45° with respect to the surface normal. The analyzer axis was also located at 45° with respect to the surface normal. For high-resolution XPS spectra, the analyzer pass energy was 23.5 eV and the energy step size was 0.1 eV. XPS quantification was based using the Multiline software [31] on the In 3d, In 3p, Ga 2p, Ga 3s, N 1s, C 1s and O 1s binding-energy regions. XPS depth profiles were obtained using 2 keV Ar^+ beam with normal incidence rastered over a 2 mm × 2 mm surface area. The Ar^+ sputter rate was in the range 1.4–10 nm min^{-1}, as measured on a SiO_2/Si reference sample. The XPS depth profiling data were analysed using the software MultiPak (ver. 9.0.1, ULVAC-PHI).

2.4. EPES evaluation of the energy dependence of electron IMFP in InGaN compounds

The elastic electron backscattering probabilities from thick InGaN layers were measured using the MICROLAB 350 spectrometer. These measurements were accompanied with similar experiments performed for both the Ni and Au standards, i.e. the samples for which the IMFP are known. During the measurements, the electron analyzer was used at the normal angle of incidence and the angle between its entrance and the surface normal was 60°. The external acceptance half-angle of the analyzer was 10° but its internal acceptance half-angle was changeable in the angle range 3°–7°. Relative EPES measurement procedures applied in the present work were already described in details elsewhere [26,29]. The electron energy dependence of the IMFP for the actual InGaN surface composition was determined within the energy range 500–2000 eV. Prior to EPES measurements, both the InGaN sample and microcrystalline mirror Ni or Au sample were *in situ* sputter-cleaned by 2 keV Ar^+ ions (at the incidence angle of 30° with respect to surface normal) until no evidence for surface contamination was detected in AES/XPS analysis. The surface cleanliness of the studied sample and standard material was also monitored after the EPES measurements.

3. Results and discussion

3.1. Surface composition and chemistry of the as-grown InGaN compounds

As-grown $In_xGa_{1-x}N$ samples of various In contents (x = 0.165 and 0.353) were analysed by XPS. An exemplary survey XPS spectrum for the as-grown $In_{0.165}Ga_{0.835}N$ layer, as determined by XRD, is shown in Fig. 1. From this spectrum, fifteen photoelectron lines (In 4p, In 4s, In $3d_{5/2}$, In $3d_{3/2}$, In 3s, In $3p_{3/2}$, In $3p_{1/2}$, Ga 3p, Ga 3s, Ga $2p_{3/2}$, Ga $2p_{1/2}$, Ga 2s, N 1s, C 1s, O 1s) were selected for quantitative analysis. The elemental atomic concentrations data on surfaces of $In_{0.165}Ga_{0.835}N$ and $In_{0.353}Ga_{0.647}N$ as-grown layers are listed in Table 1 and the calculated In/Ga, N/In, N/Ga, and N/In + Ga atomic ratios are given in Table 4. In addition, In concentrations at the as-grown layer surfaces are shown in Table 2. XPS quantitative analysis showed that the surface of all as-grown InGaN layers was contaminated with oxygen (up to 16 at.%), and with carbon (up to 9 at.%). The In/Ga, N/In, N/Ga and N/In + Ga atomic ratios of both the $In_{0.165}Ga_{0.835}N$ and $In_{0.353}Ga_{0.647}N$ layers were about

Table 1
Surface composition (in at.%) of the as-grown Ga-rich $In_xGa_{1-x}N$ layers (In bulk content x = 0.165 and 0.353).

Bulk composition	In	Ga	N	C	O
$In_{0.165}Ga_{0.835}N$	10.4	31.9	31.6	9.2	16.9
$In_{0.353}Ga_{0.647}N$	10.7	35.8	34.3	3.3	15.9

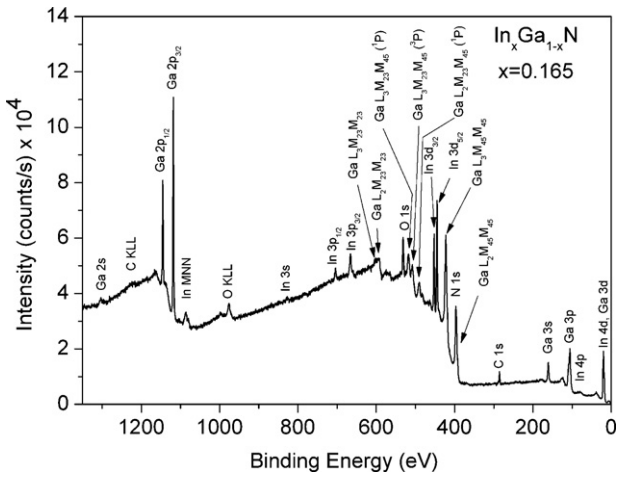

Fig. 1. The XPS survey spectrum of the as-grown $In_xGa_{1-x}N$ layer ($x = 0.165$) acquired using PHI 5000 VersaProbe™ spectrometer.

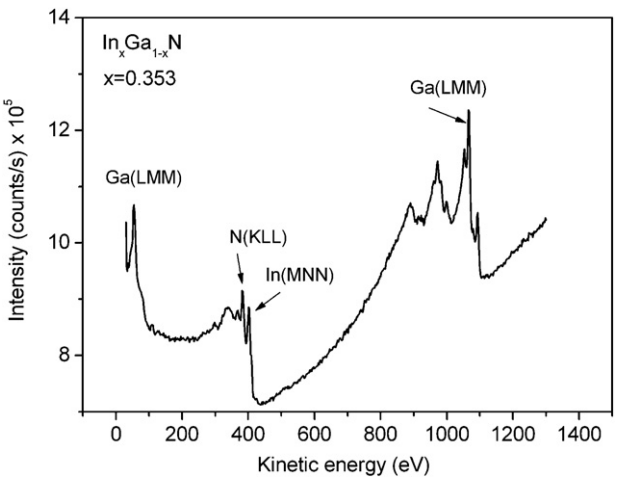

Fig. 2. The AES spectrum of the $In_xGa_{1-x}N$ layer ($x = 0.353$) acquired using MICROLAB 350 spectrometer prior to EPES measurements.

0.3, 3, 1 and 0.75 (Table 4), respectively, indicating that their surface was Ga- and N rich. As shown in Fig. 1, the N 1s XPS peak partially overlaps the Auger Ga MNN peak. As result a slight overestimation of the nitrogen surface contents can be observed what can implicate lowering of surface concentration of indium. In fact, indium surface contents are calculated to be only about 10 at.% (see Tables 1 and 2) what is much lower than the bulk In content ($x = 16.5$ and 35.3 at.%, as determined by XRD). However, the lower In surface concentration in the as-grown InGaN samples can also be explained by possible inhomogeneous distribution of In and Ga atoms [9,32].

The surface chemical states of PAMBE-grown InGaN layers were also studied with XPS. For this analysis, the In $3d_{5/2}$, Ga $2p_{3/2}$, N 1s, C 1s, and O 1s photoelectron peaks were selected. Based on the XPS analysis, an assignment of the photoelectron peaks to various chemical states of the as-grown $In_{0.165}Ga_{0.835}N$ and $In_{0.353}Ga_{0.647}N$ components is presented in Table 5. The In $3d_{5/2}$ peak can be deconvoluted into three peaks, i.e. metallic In at BE = 444.0 eV [33], indium bonded oxygen in the oxide In_2O_3 form at BE = 444.6 eV [33], and indium nitride bonded oxygen, forming the complex oxide InN_xO_y, at BE = 445.6 eV [33,34]. In contrast to the as-grown $In_{0.165}Ga_{0.835}N$ layer, we do not detect the metallic indium at the surface of $In_{0.353}Ga_{0.647}N$ layer. The Ga $2p_{3/2}$ peak analysis allow distinguish two chemical states of gallium: metallic Ga at BE = 1116.1 eV [35], and gallium bonded oxygen in the oxide Ga_2O_3 form at BE = 1118.1 eV [35,36]. The N 1s peak can be decomposed into four components resulting nitrogen bonded to gallium (GaN) at BE = 397.3 eV [34,37], nitrogen bonded to hydrogen forming NH_3 ($x < 3$) at BE = 398.5 eV [34,38], nitrogen bonded to oxygen (NO_3) at BE = 399.7 eV [34], and nitrogen bonded to hydrogen forming NH_3 at BE = 401.3 eV [34]. Three components of O 1s peak have the BE located at 530.5, 531.3 and 532.4 eV, which can be assigned to oxygen bonded to indium (In_2O_3) or gallium (Ga_xO_y) [33,39], oxygen bonded to gallium forming Ga_2O_3 [33], and oxygen bonded to nitrogen in the NO_3 form, respectively. For the as-grown $In_{0.353}Ga_{0.647}N$ layer, the O 1s peak shifts towards larger BE for about 0.5 eV.

Careful XPS analysis of oxidation states of In, Ga and N on the as-grown InGaN layer surfaces reveal composition of native oxides In_2O_3, InN_xO_y, Ga_xO_y, Ga_2O_3, and NO_3 in addition to the main Ga_2O_3 component.

Table 2
Change in the indium surface concentration (in at.%) determined by XPS/AES analyses of the as-grown Ga-rich $In_xGa_{1-x}N$ layers (In bulk content $x = 0.165$ and 0.353 are estimated from the XRD analysis) under low-energy Ar^+ ion bombardment. Quantification of XPS and AES data was performed using Multiline [31] and Avantage softwares, respectively.

In bulk concentration (at.%)	Treatment	In surface concentration (at.%)	
XRD		XPS	AES
16.5	As-grown	10.4	–
	1 keV Ar^+-sputtered	–	11.3
	2 keV Ar^+-sputtered	6.6	–
35.3	As-grown	10.7	–
	1 keV Ar^+-sputtered	–	19.5
	2 keV Ar^+-sputtered	7.8	–

Table 3
Surface composition (in at.%) of the Ga-rich $In_xGa_{1-x}N$ layers (In bulk content $x = 0.165$ and 0.353) after 2 keV Ar^+ ion-sputtering.

Bulk composition	In	Ga	N	C	O
$In_{0.165}Ga_{0.835}N$	6.6	63.2	25.9	–	4.3
$In_{0.353}Ga_{0.647}N$	7.8	63.5	25.3	–	3.5

3.2. Surface composition and chemistry of the InGaN compounds under Ar-ion sputtering

In order to get better insight in chemical surface composition of as grown InGaN layers, we applied a short time Ar^+ sputtering procedure to remove carbon-like surface contaminants. Both AES and XPS were used for surface analysis of such sputter-cleaned InGaN layers.

Fig. 2 shows the Auger spectrum from the $In_{0.353}Ga_{0.647}N$ layer after 2 keV Ar-ion sputtering and before EPES measurements. The indium and other elemental concentrations (in at.%), and the In/Ga, N/In, N/Ga, and N/In + Ga atomic ratios at the surface sputtered with Ar^+ ions of both $In_{0.165}Ga_{0.835}N$ and $In_{0.353}Ga_{0.647}N$ layers are shown in Tables 2–4. The presented results show that Ar^+ sputtering removes efficiently the whole carbon adsorbed on the surface,

Table 4
Atomic ratios of In/Ga, N/In, N/Ga, and N/In + Ga in surface region of the Ga-rich $In_xGa_{1-x}N$ layers (In bulk content $x = 0.165$ and 0.353) prior to and after 2 keV Ar^+ ion-sputtering.

Bulk composition	Treatment	In/Ga	N/In	N/Ga	N/In + Ga
$In_{0.165}Ga_{0.835}N$	As-grown	0.33	3.04	0.99	0.75
	Sputtered	0.10	3.92	0.41	0.37
$In_{0.353}Ga_{0.647}N$	As-grown	0.30	3.20	0.96	0.74
	Sputtered	0.12	3.24	0.40	0.35

Table 5
Binding energies (BE) and relative spectral areas obtained from the fit of the XPS spectra recorded from the as-grown Ga-rich $In_xGa_{1-x}N$ layers (In bulk content $x = 0.165$ and 0.353).

Sample	Element	Core level	BE (eV)	Relative spectral area (%)	Assignment
$In_{0.165}Ga_{0.835}N$	In	$3d_{5/2}$	444.0	5	Metallic In
		$3d_{5/2}$	444.6	48	In_2O_3
		$3d_{5/2}$	445.6	47	InN_xO_y
	Ga	$2p_{3/2}$	1116.1	2	Metallic Ga
		$2p_{3/2}$	1118.1	98	Ga_2O_3
	N	1s	397.3	27	GaN
		1s	398.5	6	NH_x ($x < 3$)
		1s	399.7	2	NO_3
		1s	401.3	1	NH_3
	C	1s	285.0	100	–CH
	O	1s	530.5	34	In_2O_3, Ga_xO_y
		1s	531.3	52	Ga_2O_3
		1s	532.4	14	NO_3
$In_{0.353}Ga_{0.647}N$	In	$3d_{5/2}$	444.6	77	In_2O_3
		$3d_{5/2}$	445.6	23	InN_xO_y
	Ga	$2p_{3/2}$	1116.4	4	Metallic Ga
		$2p_{3/2}$	1118.3	96	Ga_2O_3
	N	1s	397.2	28	GaN
		1s	398.2	9	NH_x ($x < 3$)
		1s	399.2	3	NO_3
		1s	400.6	2	NH_3
	C	1s	285.0	100	–CH
	O	1s	531.0	57	In_2O_3, Ga_xO_y
		1s	531.8	35	Ga_2O_3
		1s	533.1	8	NO_3

leaving a small (about 4 at.%) concentration of oxygen contamination. However, the Ar^+ sputtering removes also partially the surface In and N atoms, causing the formation of Ga rich surface. As result, the atomic ratios of In/Ga, N/Ga and N/In + Ga become lower and the N/In ratio increases, especially for the $In_{0.165}Ga_{0.835}N$ layer (Table 4). For the $In_{0.353}Ga_{0.647}N$ layer, the latter value slightly increases from 3.20 prior to sputtering to 3.24 after 1 min sputtering time (Table 4).

The Ar^+ sputter-induced rearrangement of surface composition accompanied by metallic gallium appearance was observed by Chang et al. [40]. The GaInN surface exposed to the 2 keV Ar^+ ion beam was found to be preferentially sputtered [41]. Such phenomenon was observed also for GaN, where the Ar ion bombardment caused preferential depletion of nitrogen from the surface [27,42], resulting in a Ga-rich surface. A preferred loss of In with respect to Ga can also be explained [43,44] by much lower bond energy of InN (7.7 eV/atom) than GaN (8.9 eV/atom).

Careful analysis of elemental core-level XPS spectra was carried out to characterize the chemical nature of components on Ar^+ sputter-cleaned InGaN layers. Table 6 shows the binding energies and relative spectral areas of convoluted peaks fitting all considered photoelectron lines, and their chemical assignment. The chemical rearrangement of the InGaN layer due to Ar^+ etching is evidenced by direct comparison of the XPS data taken before (Table 5) and after (Table 6) Ar^+ sputter-cleaning. From Table 6 is visible that after argon ion bombardment, the XPS peak associated with indium and gallium oxides diminish and contributions of metallic In and GaN are emerged in the In $3d_{5/2}$ and Ga $2p_{3/2}$ photoelectron lines, respectively at BE = 443.8 eV [39] and BE = 1116.8 eV [34], respectively. Generally, the XPS results for argon-bombarded InGaN layers

Table 6
Binding energies (BE) and relative spectral areas obtained from the fit of the XP spectra recorded after 2 keV Ar^+ ion-sputtering of Ga-rich $In_xGa_{1-x}N$ layers (In bulk content $x = 0.165$ and 0.353).

Sample	Element	Core level	BE (eV)	Relative spectral area (%)	Assignment
$In_{0.165}Ga_{0.835}N$	In	$3d_{5/2}$	443.8	58	Metallic In
		$3d_{5/2}$	444.6	34	In_2O_3
		$3d_{5/2}$	445.5	8	InN_xO_y
	Ga	$2p_{3/2}$	1116.9	79	GaN
		$2p_{3/2}$	1118.3	21	Ga_2O_3
	N	1s	397.0	17	GaN
		1s	398.2	3	NH_x ($x < 3$)
		1s	399.7	1	NO_3
	O	1s	530.8	72	In_2O_3, Ga_xO_y
		1s	532.4	28	NO_3
$In_{0.353}Ga_{0.647}N$	In	$3d_{5/2}$	443.8	59	Metallic In
		$3d_{5/2}$	444.5	34	In_2O_3
		$3d_{5/2}$	445.4	7	InN_xO_y
	Ga	$2p_{3/2}$	1116.8	79	GaN
		$2p_{3/2}$	1118.2	21	Ga_2O_3
	N	1s	396.9	17	GaN
		1s	398.0	3	NH_x ($x < 3$)
		1s	399.3	1	NO_3
	O	1s	530.4	38	In_2O_3, Ga_xO_y
		1s	531.2	38	Ga_2O_3
		1s	532.6	24	NO_3

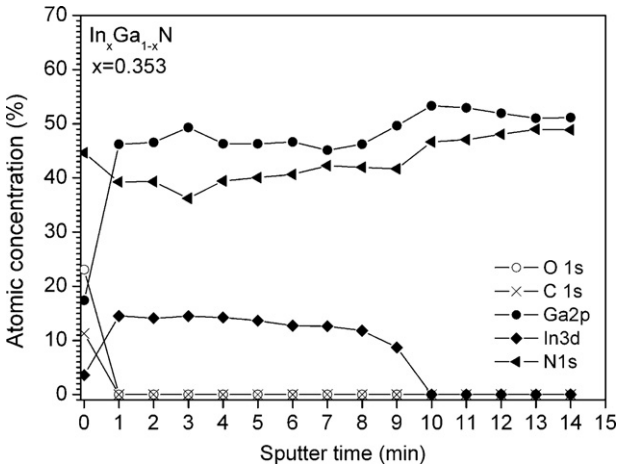

Fig. 3. The XPS sputter depth profiles of the $In_xGa_{1-x}N$ layer ($x = 0.353$). The relative atomic concentration depth distribution of oxygen, carbon, gallium, indium and nitrogen evaluated from the O 1s, C 1s, Ga 2p, In 3d, and N 1s XPS peaks, respectively, are shown as a function of sputter time (a sputter rate is 10 nm min^{-1} relative to a 100-nm-thick SiO_2/Si layer).

(Table 6) evidence the presence of the native oxide, consisting of the group III elements-O, In–N–O, N–O and N–H species, on GaN compound with metallic In content.

In order to examine the bulk composition of the InGaN layers, we used the XPS depth profiling technique, which allows evaluate the relative atomic concentration of oxygen, carbon, gallium, indium and nitrogen in depth of sample as a function of sputter time. The result of such analysis is presented in Fig. 3. The depth-profiles of all elements indicate that the 100 nm thick $In_{0.353}Ga_{0.647}N$ layer can be considered as a homogeneous layer within an analytical area. Carbon and oxygen contents decrease rapidly in the depth of about 10 nm, and then remain undetectable. The In, Ga and N atomic concentrations are rather constant throughout the layer.

3.3. Inelastic mean free path of 500–2000 eV electrons in the InGaN compounds

Prior to EPES measurements, the $In_xGa_{1-x}N$ compounds were sputter-cleaned using 2 keV Ar^+ ions etching for 1 min. Following this procedure, only a small amount of oxygen was detected by XPS on the InGaN compound surface.

The IMFP values for these compounds were determined for electron energies of 500–2000 eV. The values obtained using relative EPES measurements are shown in Fig. 4(a) and Table 7, together with IMFPs calculated using the TPP-2M predictive formula [24] for both compounds. For comparison, Fig. 4(b) shows also the measured and calculated IMFPs published in Ref. [27] for binary GaN single crystal. The TPP-2M formula [24] for predicting the IMFP, λ, as a function of electron energy, E (in eV) is

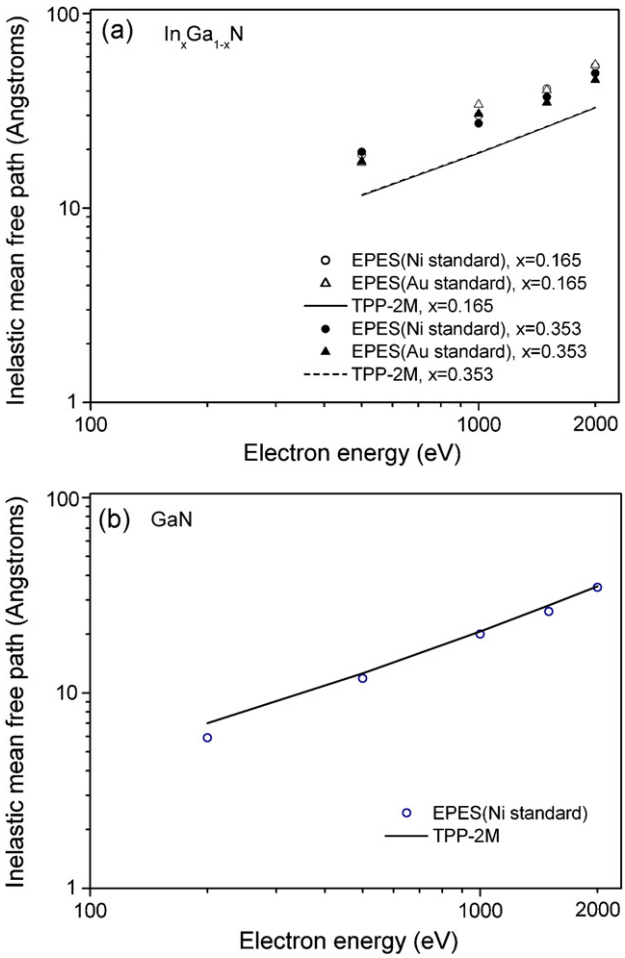

Fig. 4. Comparison of measured and predicted IMFPs for the two nitrides, containing GaN compound, as a function of electron energy: (a) the actually studied ternary $In_xGa_{1-x}N$ layers ($x = 0.165$ and 0.353); (b) the recently studied bulk GaN single crystal [27]. Symbols show measured IMFPs using the relative EPES measurements. Lines represent IMFPs predicted from the TPP-2M equation [24].

$$\lambda = \frac{E}{E_p^2[\beta \ln(\gamma E) - (CE) + (DE^2)]} \quad (1)$$

$$E_p = 28.8\sqrt{\frac{N_v \rho}{M}} \quad (1a)$$

Table 7
EPES-measured and TPP-2M IMFP values predicted from Eq. (1) for Ga-rich $In_xGa_{1-x}N$ layers (In bulk content $x = 0.165$ and 0.353). RMS and R deviations from TPP-2M, calculated using Eq. (2), are shown in separate columns. EPES IMFP, RMS and R values in the brackets are related to the Au standard while the other values correspond to the Ni standard.

Bulk composition	Energy (keV)	IMFPs (Å)		Deviation from TPP-2M	
		EPES	TPP-2M	RMS (Å)	R (%)
$In_{0.165}Ga_{0.835}N$	0.5	18.8(17.2)	11.6		
	1	30.0(34.1)	19.2		
	1.5	41.1(40.6)	26.2		
	2	53.8(54.5)	32.8		
				14.4(15.2)	59.8(61.7)
$In_{0.353}Ga_{0.647}N$	0.5	19.5(17.4)	11.7		
	1	27.3(30.6)	19.3		
	1.5	37.3(34.9)	26.3		
	2	49.5(45.6)	33.0		
				11.4(9.9)	50.0(44.5)

where E_p is the free-electron plasmon energy (in eV), N_v is the number of valence electrons per atom or molecule (for InGaN), ρ is the density (in g cm^{-3}), M is the atomic or molecular weight while β, γ, C and D are material-dependent parameters. These parameters are correlated to simple material properties like the band-gap energy E_g, ρ, and a valence electron density parameter $U = N_v\rho/M$. Values of the four parameters β, γ, C and D are calculated from Eqs. (4a)–(4d) published in Ref. [24]. For the $In_{0.165}GaN$ and $In_{0.353}GaN$ nitrides, values of E_g, E_p, and ρ are 2.75 and 2.08 eV, 21.3 and 20.6 eV, and 6.26 and 6.38 g cm^{-3}, respectively. For these nitrides $N_v = 8$ is calculated from the sum of contributions from each constituent element (i.e., N_v for each element multiplied by the stoichiometric coefficient for that element) [23].

On close inspection of Fig. 4 and Table 7, we notice that the EPES IMFP values in $In_{0.165}Ga_{0.835}N$ and in $In_{0.353}Ga_{0.647}N$ are similar, however, they are larger than the IMFPs for GaN. Considerable deviation between the measured and predicted IMFPs can be ascribed to a different structure of currently studied samples than the structure of the GaN crystal. The measured IMFPs for InGaN samples seem to be reliable since they were obtained from measurements involving two standards. It seems that the deviation of the measured IMFPs from the predicted IMFPs can be largely ascribed to the TPP-2M formula [24]. One should stress the fact that in the derivation of the TPP-2M, no IMFP data for inorganic compounds were used.

To compare numerically the EPES-determined IMFPs without corrections for surface excitations with the corresponding predicted IMFPs, a statistical analysis of the data was made using the root-mean-square deviation (RMS) and the mean percentage deviation (R). These parameters were calculated from

$$\mathrm{RMS} = \sqrt{\frac{1}{r}\sum_{n=1}^{r}(\lambda_n - \lambda_{\mathrm{theory}})^2}$$

$$R = 100\frac{1}{r}\sum_{n=1}^{r}\left|\frac{\lambda_n - \lambda_{\mathrm{theory}}}{\lambda_{\mathrm{theory}}}\right| \quad (2)$$

where r is the total number of experimental inelastic mean free path values λ_n uncorrected for surface excitations for $In_{0.165}Ga_{0.835}N$ and $In_{0.353}Ga_{0.647}N$ (in the present work, calculations were made for a number of IMFPs, $r = 4$) and $\lambda_{\mathrm{theory}}$ denotes the IMFP value calculated from the TPP-2M equation [24] at a particular electron energy. The RMS and R deviations resulting from Eq. (2) for the two examined InGaN layers are also shown in Table 7. The observed deviations are relatively large (see Table 7), however, they are similar for both Ni and Au standards. The smallest RMS and R deviations of 9.9 Å and 44.5%, respectively, are found between EPES IMFP data (Au standard) and those predicted using the TPP-2M (Eq. (1)) for the $In_{0.353}Ga_{0.647}N$ layer. However, it should be noted that the IMFP values resulting from EPES are strictly limited to the surface region, whereas the calculated IMFP values refer to the bulk of the solid.

For comparison, Fig. 4(b) shows the already published energy dependence of IMFP in GaN [27]. For this sample with the perfect crystal structure, the measured IMFPs are in good agreement with those predicted. Krawczyk et al. [27] have found the RMS and R values of 1.4 Å and 8.1%, respectively. These values indicate high consistency between measured and predicted IMFPs for the GaN single crystal.

It seems that the observed discrepancies between the measured and predicted IMFPs originate from: (i) the reliability of theoretical model of electron transport used in EPES method for ternary nitrides, (ii) the accuracy of the input parameters used in EPES method (e.g. IMFP value for the standard material, sample density, and elastic scattering cross sections) and (iii) the higher level of compositional and structural imperfections present in the InGaN thick layers. Based on the obtained results, we may expect that the major contribution to the inaccuracies in EPES IMFPs is rather the lack of accuracy of the presently available models for elastic electron scattering in ternary nitride layers with the low crystalline quality, and the inhomogeneous distribution of In content in the layer.

4. Conclusions

The present AES-XPS study provided new experimental data related to compositional and chemical characterization of InGaN thick layer surfaces, and could be useful in solving key issues associated with the growth of high-quality layer with much higher In content. From the XPS multiline analysis, the surface atomic content of indium was found to be only about 10 at.% ($x = 0.1$). This value is much lower than the corresponding bulk value ($x = 0.165$ and 0.353) determined from the XRD measurement. Mostly, such In-deficient surface is formed as result of inhomogeneous distributions of In in the thick InGaN microstructures of the low crystalline quality. However, the composition of examined layers, as determined by XPS depth profiling analysis, was found to be uniform over a 100 μm × 100 μm area in bulk of thick layers. The as-grown InGaN layer surface was covered by native oxides (In_2O_3, InN_xO_y, Ga_xO_y, Ga_2O_3, and NO_3), and contaminants originated from carbon-like species. Good agreement was obtained between quantification of surface elemental composition from XPS and AES spectra.

The content of surface carbon and oxygen contaminants, as well as indium and nitrogen components, was efficiently reduced after 2 keV Ar^+ sputtering. However, the argon-ion etching induced also formation of Ga-rich surface with metallic indium and nitride-based components.

The EPES measurements applied without corrections for surface excitations, involving the Ni and Au standards, were found to be a useful method for determination of the IMFP in the examined layers. The experimental IMFPs were larger than those calculated from the TPP-2M equation [24]. These differences may be accounted for, at least partially, by the compositional and structural imperfection of the InGaN compound.

Acknowledgements

This work was partially supported by the European Union within European Regional Development Fund, through grant Innovative Economy (POIG.01.01.02-00-008/08), and by the MNiSW grant no. N N204 0769 33.

References

[1] O. Jani, I. Ferguson, Ch. Honsberg, S. Kurtz, Appl. Phys. Lett. 91 (2007) 132117–132123.
[2] M. Shimizu, Y. Kawaguchi, K. Hiramatsu, N. Sawaki, Jpn. J. Appl. Phys. 36 (1997) 3381–3384.
[3] E.L. Piner, F.G. McIntosh, J.C. Roberts, K.S. Boutros, M.E. Aumer, V.A. Joshkin, N.A. El-Masry, S.M. Bedair, S.X. Liu, Materials Research Society Symposium Proceedings 449, 1997, p. 85.
[4] V.P. Chaly, B.A. Borisov, D.M. Demidov, D.M. Krasovitsky, Yu.V. Pogorelsky, A.P. Shkurko, I.A. Sokolov, S.Yu. Karpov, J. Cryst. Growth 206 (1999) 147–149.
[5] R. Singh, D. Doppalapudi, T.D. Moustakas, L.T. Romano, Appl. Phys. Lett. 70 (1997) 1089–1091.
[6] G.B. Stringfellow, J. Cryst. Growth 312 (2010) 735–749.
[7] J. Adhikari, D.A. Kofke, J. Appl. Phys. 95 (2004) 4500–4502.
[8] L.K. Teles, M. Marque, L.M.R. Scolfaro, J.R. Leite, Braz. J. Phys. 34 (2004) 593–597.
[9] H. Chen, R.M. Feenstra, J.E. Northrup, T. Zywietz, J. Neugebauer, Phys. Rev. Lett. 85 (2000) 1902–1905.
[10] S.J. Pearton, J.C. Zolper, R.J. Shul, F. Ren, J. Appl. Phys. 86 (1999) 1–78.
[11] M.A. Reshchikov, H. Morkoc, J. Appl. Phys. 97 (2005) 061301–061395.
[12] O. Ambacher, J. Phys. D: Appl. Phys. 31 (1998) 2653–2710.
[13] B. Monemar, P.P. Paskov, A. Kasic, Superlattices Microstruct. 38 (2005) 38–56.
[14] A.G. Bhuiyan, A. Hashimoto, A. Yamamoto, J. Appl. Phys. 94 (2003) 2779–2808.
[15] Y. Nanishi, Y. Saito, T. Yamaguchi, Jpn. J. Appl. Phys. 42 (2003) 2549–2559.
[16] F.K. Yam, Z. Hassan, Superlattices Microstruct. 43 (2008) 1–23.

[17] T. Matsuoka, Superlattices Microstruct. 37 (2005) 19–32.
[18] M. Kurouchi, T. Araki, H. Naoi, T. Yamaguchi, A. Suzuki, Y. Nanishi, Phys. Status Solidi (b) 241 (2004) 2843–2848.
[19] A. Jablonski, Surf. Sci. 603 (2009) 1342–1352.
[20] Surface Chemical Analysis – Vocabulary, ISO 18115, International Organisation for Standardisation, Geneva, 2001.
[21] Standard Terminology Relating to Surface Analysis, ASTM E673-03, Annual Book of ASTM Standards, 2006, vol. 3.06, ASTM International, West Conshohocken, 2006, p. 647.
[22] C.J. Powell, A. Jablonski, J. Phys. Chem. Ref. Data 28 (1999) 19–62.
[23] C. J. Powell, A. Jablonski, NIST ELECTRON INELASTIC-MEAN-FREE-PATH DATABASE, Version 1.1, Standard Reference Data Program Database 71, U.S. Department of Commerce, National Institute of Standards and Technology, Gaithersburg, MD, 2000 (http://www.nist.gov/srd/nist71.htm).
[24] S. Tanuma, C.J. Powell, D.R. Penn, Surf. Interface Anal. 21 (1994) 165–176.
[25] G. Gergely, Surf. Interface Anal. 3 (1981) 201–205.
[26] A. Jablonski, Surf. Interface Anal. 37 (2005) 1035–1044.
[27] M. Krawczyk, L. Zommer, A. Jablonski, I. Grzegory, M. Boćkowski, Surf. Sci. 566–568 (2004) 1234–1239.
[28] M. Krawczyk, L. Zommer, A. Kosiński, J.W. Sobczak, A. Jablonski, Surf. Interface Anal. 38 (2006) 644–647.
[29] M. Krawczyk, A. Kosiński, A. Jablonski, A. Mycielski, Surf. Sci. 600 (2006) 3744–3748.
[30] M. Siekacz, A. Feduniewicz-Żmuda, G. Cywiński, M. Kryśko, I. Grzegory, S. Krukowski, K.E. Waldrip, W. Jantsch, Z.R. Wasilewski, S. Porowski, C. Skierbiszewski, J. Cryst. Growth 310 (2008) 3983–3986.
[31] A. Jablonski, Anal. Sci. 26 (2010) 155–164.
[32] J. Wu, J. Appl. Phys. 106 (2009) 011101–11128.
[33] G. Hollinger, R. Skheyta-Kabbani, M. Gendry, Phys. Rev. B 49 (1994) 1159–1167.
[34] J.F. Moulder, W.F. Stickle, P.E. Sobol, K.D. Bomben, Handbook of X-ray Photoelectron Spectroscopy, ULVAC-PHI, Inc./Physical Electronics USA, Inc., Chigasaki 253-8522 Japan/MN 55317, USA, 1995.
[35] C.C. Surdu-Bob, S.O. Saied, J.L. Sullivan, Appl. Surf. Sci. 183 (2001) 126–136.
[36] W. Priyantha, G. Radhakrishnan, R. Droopad, M. Passlack, J. Cryst. Growth 323 (2011) 103–106.
[37] K. Li, Z.C. Feng, C.-C. Yang, Int. J. Nanosci. 3 (2004) 655–661.
[38] L. Kubler, E.K. Hill, D. Bolmont, J.C. Peruchetti, Thin Solid Films 149 (1987) 385–392.
[39] S. Krischok, V. Yanev, O. Balykov, M. Himmerlich, J.A. Schaefer, R. Kosiba, G. Ecke, I. Cimalla, V. Cimalla, O. Ambacher, H. Lu, W.J. Schaff, L.F. Eastman, Surf. Sci. 566–568 (2004) 849–855.
[40] C.-A. Chang, C.-F. Shih, N.-C. Chen, T.Y. Lin, K.-S. Liu, Appl. Phys. Lett. 85 (2004) 6131–6133.
[41] S.J. Pearton, C.R. Abernathy, F. Ren, J.R. Lothian, J. Appl. Phys. 76 (1994) 12101–21215.
[42] J. Kovac, A. Zalar, Surf. Interface Anal. 34 (2002) 253–256.
[43] J.E. Northrup, J. Neugebauer, L.T. Romano, Appl. Phys. Lett. 74 (1999) 2319–2321.
[44] J.E. Northrup, J. Neugebauer, Phys. Rev. B60 (1999) R8473–R8476.